Electromigration Simulation of Copper-Pillar Bump in 3D Integration

Du, Zhoubang; Du, Leiming; Zhang, Guo Qi

DOI
10.1109/EuroSimE65125.2025.11006578

Publication date
2025

Document Version
Final published version

Published in
Proceedings - 2025 26th International Conference on Thermal, Mechanical and Multi-Physics Simulation and Experiments in Microelectronics and Microsystems, EuroSimE 2025

2025 26th International Conference on Thermal, Mechanical and Multi-Physics Simulation and Experiments in Microelectronics and Microsystems (EuroSimE) | 979-8-3503-9300-2/25/$31.00 ©2025 IEEE | DOI: 10.1109/EUROSIME65125.2025.11006578

Electromigration Simulation of Copper-Pillar Bump in 3D Integration

1st Zhoubang DU
EEMCS Faculty
Delft University of Technology
Delft, the Netherlands
zhoubangdu@tudelft.nl

2nd Leiming Du
EEMCS Faculty
Delft University of Technology
Delft, the Netherlands
l.du@tudelft.nl

3rd GuoQi Zhang
EEMCS Faculty
Delft University of Technology
Delft, the Netherlands
g.q.zhang@tudelft.nl

***Abstract*—The continuous trend toward miniaturization and increased integration density in semiconductor devices has exacerbated electromigration (EM) issue, making it a significant reliability concern in advanced packaging technologies, especially in copper (Cu)-pillar bumps used in 3D integration. This study investigates the EM phenomenon in a Cu-pillar bump structure using the birth/death element method in ANSYS. The model incorporates electro-thermal-structural-diffusion coupling transient simulations to analyze the time-dependent evolution of atomic concentration and resistance under varying experimental durations, model sizes, temperatures and current. The simulation results indicate that increased current and temperature significantly accelerate the formation of voids, leading to earlier EM failure. A comparative study between forward and inverse current reveals differences in the evolution of EM-induced damage, where inverse currents exhibiting lower resistance growth over time. These findings provide valuable insights into the design of Cu-pillar bump structures to enhance EM resistance in advanced packaging technologies.**

***Index Terms*—Birth/Death Element Method, Finite Element Simulation, EM, 3D Integration**

I. INTRODUCTION

As semiconductor manufacturing processes continue to evolve to smaller nodes, traditional packaging technologies are gradually struggling to meet the demands for high performance and high density. Advanced packaging technologies, such as 2.5D packaging, 3D integrated packaging, and system-in-package (SiP), have become key solutions for achieving higher functional integration and system performance. As a key interconnect material in packaging, solder material is not only responsible for the electrical connection between the chip and the package substrate but also plays the role of mechanical support and heat dissipation. Electromigration (EM) effect refers to the migration of atoms in conductive metals under high current density conditions due to electron wind force. This phenomenon can lead to localized voids, cracks or metal aggregation in the solder material, which in turn causes electrical connection failure, seriously threatening the stability and lifetime of electronic devices. In advanced packaging structures, the resulting increase in current density and heat flux density due to the miniaturization of the solder bump and pitch can cause serious EM failure issues [1], [2], especially in microbumps, which are more susceptible to EM effects.

This paper analyzes the EM phenomenon of a copper (Cu)-pillar bump structure by using the birth/death element method. The EM phenomenon occurs at the contact surface between the SnAg1.8 solder bump and the Cu pillar. In ANSYS, a layer of birth/death element is used for the electro-thermal-structural-diffusion coupling transient simulation method. By analyzing the time-dependent curves of atomic concentration and resistance at a critical concentration level, the impact of the EM phenomenon on the contact surface was predicted under varying model sizes, time, temperatures and current. In the next part of the paper, section II introduces the methodology used in this simulation, section III gives the simulation results and discussions under different experimental conditions, section IV conducts some experiments to verify the simulation results, and section 5 gives the conclusion of this simulation.

II. METHODOLOGY

A. Migration model

The electro-thermal-structural-diffusion coupled model is used in this paper, to simulate hydrostatic stress migration, thermal migration, and EM effects in diffusion analysis, coupled to structural, thermal, and electrical degrees of freedom, respectively. These combined effects can be used to simulate the EM of atoms or vacancies in metallic interconnects.

The total atomic flux of EM can be written as:

$$J_a = -[D]\nabla C - \frac{[D]CZ^*e\nabla\varphi}{kT} + \frac{[D]C\Omega\nabla\sigma_H}{kT} - \frac{[D]CQ\nabla T}{kT^2}$$

[3]

where

- $[D]$ is the atomic diffusivity matrix,
- C is the atomic concentration,
- Z^* is the effective charge number of the atom that combines the effects of the electrostatic and the electron wind forces,
- e is the elementary charge
- φ is the electric potential,
- k is Boltzmann's constant,
- T is the absolute temperature,
- Ω is the atomic volume,
- Q is the heat of atomic transport

979-8-3503-9300-2/25/$31.00 ©2025 IEEE Presented at the EuroSimE 2025 Conference

- The hydrostatic stress is defined as the average of principal stresses ($\sigma_H = (\sigma_{11} + \sigma_{22} + \sigma_{33})/3 = \mathrm{tr}(\sigma_{ij})/3$), where tr denotes the trace operator.

It is worth mentioning that the temperature gradient can be disregarded due to the microscale of the dimensions.

B. Birth/Death element method

The birth/death element method is a finite element simulation technique widely used in ANSYS to simulate complex processes involving the gradual addition or removal of materials.

To dynamically adjust the state of simulation objects, the birth/death method performs:

- Birth: Reactivate the unit and restore its original physical properties to simulate the addition of material.
- Death: Reduce the physical properties of the unit to an extremely low level, thereby effectively removing its influence on the global system and simulating the removal of material.

Due to high flexibility and high computational efficiency in dynamic simulation, this method is particularly suitable for describing phenomena such as material deposition, removal or failure. It has significant flexibility and computational efficiency and is widely used in the simulation of electronic packaging [4]–[7], such as the simulation of the warpage evolution of wafer-level chip packaging (WLCSP), the simulation of the laser bonding packaging process of organic light-emitting diodes (OLEDs), the stress redistribution analysis during the acid corrosion depackaging process, and the analysis of thermal deformation during reflow soldering of power devices.

III. SIMULATION

In this section, a cross-section of the geometry used in the simulation is shown, mesh sensitivity analyzes are performed and setup conditions such as boundary conditions are given.

A. The geometry of the model

Fig. 1 shows the cross-section of the Cu-pillar bump used in the simulation.

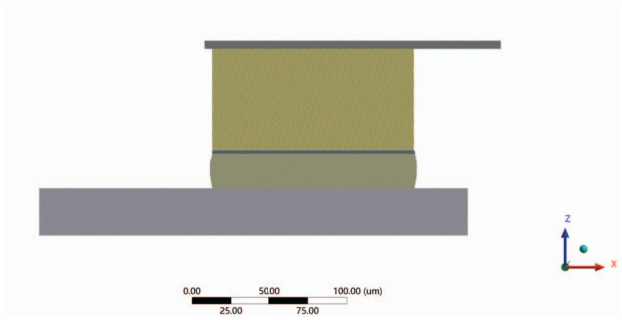

Fig. 1: Cross-section of the model.

The main structure of the model consists of a Cu pillar, top metal pad, substrate and solder bump. A layer of 2 μm is defined in the contact area between the Cu pillar and the solder bump to simulate the formation of voids where EM occurs. The upper part of the Cu pillar is an Al pad with a thickness of 5 μm, and the lower part of the solder ball is a Cu pad with a thickness of 30 μm.

B. Mesh sensitivity analysis

Mesh sensitivity analysis is a critical technique in finite element analysis, assessing the influence of mesh resolution on simulation results to determine an optimal mesh density. The finer the mesh, the higher the accuracy, but also the higher the computational cost, while too coarse a mesh may lead to large computational errors, so the choice of mesh resolution is a balance between computational cost and accuracy. The coarse mesh is chosen to realize the convergence of the simulation results, and then gradually refine the mesh and record the simulation results of the birth/death element layers, and finally, after the changes in the calculation results tend to be stable and achieve mesh independence, the medium mesh is chosen to achieve the balance of computational efficiency and accuracy. Fig. 2 shows the simulation results of the birth/death element layer with different mesh accuracy. In this simulation, the key element sizes of the birth/death element layer are chosen as 4/6/8 μm, corresponding to the fine/medium/coarse meshs, and the simulation is carried out at 2A, 140°C for 500 hours, which is also the reference of all simulations.

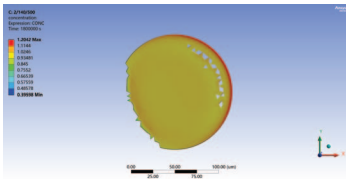

(a) 4μm

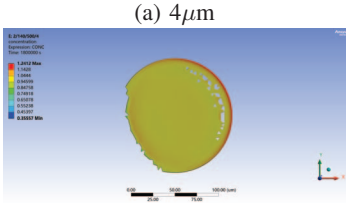

(b) 6μm

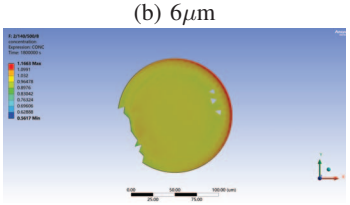

(c) 8μm

Fig. 2: Mesh in different sizes

Extracting the curves of the resistance of the birth/death element layer with time can reflect the sensitivity of the simulation results of EM phenomenon under different mesh precision. Fig. 3 displays the curves of the resistance of the birth/death element layer with time under different mesh precision, which can be seen that the resistance curves of the coarse mesh is has a large error, while the errors of

the resistance curves between the fine mesh and the selected medium mesh is acceptable.

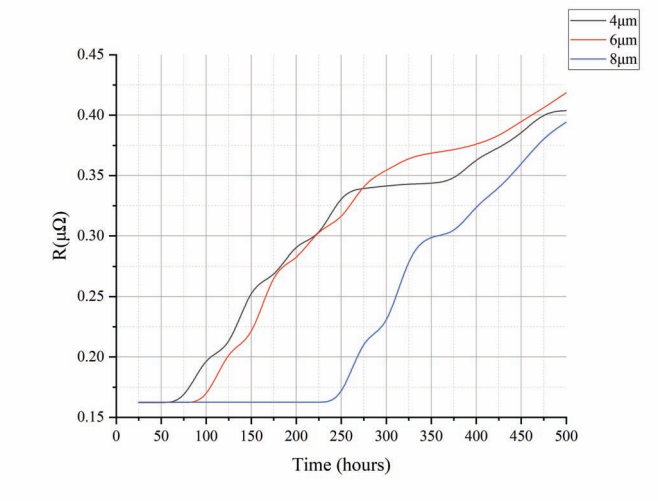

Fig. 3: Resistance with time under different mesh precision.

Mesh sensitivity analysis usually adopts the **mesh Convergence Index (GCI)** for gird independence analysis [8], which is defined as:

$$GCI = \frac{F_s|\varepsilon|}{r^p - 1} * 100\%$$

where:

- F_s is the safety factor (typically taken as 1.25 for three or more meshes).
- E is the relative error between adjacent mesh results:

$$\varepsilon = \frac{f_2 - f_1}{f_1}$$

  where f_1 and f_2 represent the computed results for the coarse mesh and fine mesh, respectively.
- r is the mesh refinement ratio:

$$r = \frac{h_1}{h_2}$$

  where h_1, h_2 are the mesh sizes (e.g., mesh element length, volume, etc.).
- p is the method order (for common second-order methods, $p \approx 2$).

Substituting the final resistance values of the fine mesh and the medium mesh after 500 hours ($0.404\,\mu\Omega$ and $0.418\,\mu\Omega$), it can be calculated that:

$$GCI = 1.4\%$$

which indicates that mesh independence has been achieved and the calculation error is acceptable.

C. Setup conditions

In this simulation, the reference temperature is set at 25°C , the thermal expansion of the material is taken into account, the atomic concentration of the birth/death layer is normalized and the total number of solution steps is set at 20 according to the time step. In each substep, when the atomic concentration of the element within the birth/death layer is lower than 0.98, it is considered to exceed the threshold value of the strain of failure and the element is therefore removed. Fig. 4 shows the constraints of the model.

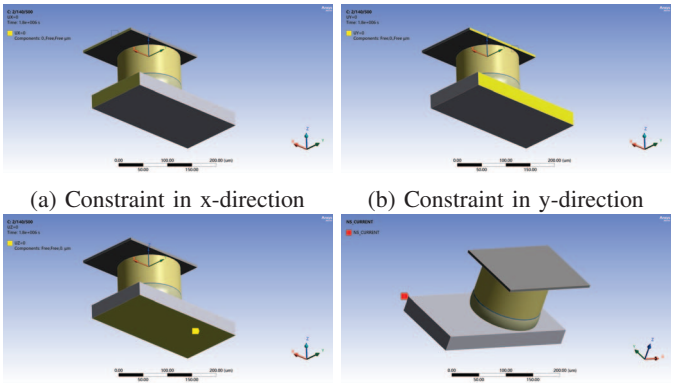

(a) Constraint in x-direction (b) Constraint in y-direction

(c) Constraint in z-direction (d) the direction of the current

Fig. 4: Constraints of the model in different directions.

IV. Results and Discussions

In this section, the simulation results of the model under different sizes, temperatures, and current are shown. The effects of different conditions on the occurrence of EM are discussed, as well as the shortcomings of this simulation and the direction of improvement.

A. Experimental durations

Fig. 5 shows the simulation results of the model at 2A, 140°C after 250/500/750/100 hours for the birth/death element layer, as the experiment proceeds, the atomic concentration of some elements reaches the threshold of the failure strain and therefore is removed. Fig. 6 shows the resistance of the birth/death element layer with time, The simulation results indicate that EM-induced void formation and atomic depletion lead to a substantial increase in resistance. Initially, EM effects are negligible, but after 80 hours, the resistance starts to increase significantly, and after 500 hours,the resistance grows from 0.1624 $\mu\Omega$ to 0.4198 $\mu\Omega$, which is a 158% increase.By reaching 1000 hours, the resistance has a 239% increase.

B. Model size

A smaller model is added to the simulation to compare with the reference model for the effect of reduced model size on the EM phenomenon. The smaller model with the same structure as the reference, consists of a Cu pillar of a diameter of $90\,\mu$m and a height of $45\,\mu$m and a SnAg1.8 solder bump with a diameter of $90\,\mu$m and a height of $20\,\mu$m. A layer of $2\,\mu$m is also defined in the contact area between the copper pillar and the solder bump.

Fig. 7 shows the simulation results of the reference and smaller model at 2A, 140°C. After 500 hours, the smaller model experienced more severe EM, with close to 1/3 of the sections failing, which demonstrates that a reduction in

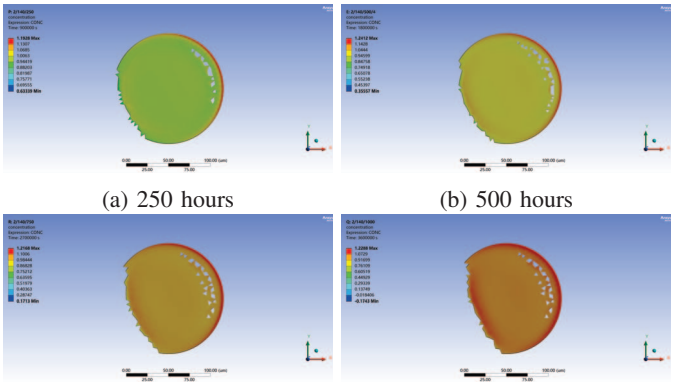

(a) 250 hours (b) 500 hours

(c) 750 hours (d) 1000 hours

Fig. 5: Simulation results over different experimental durations.

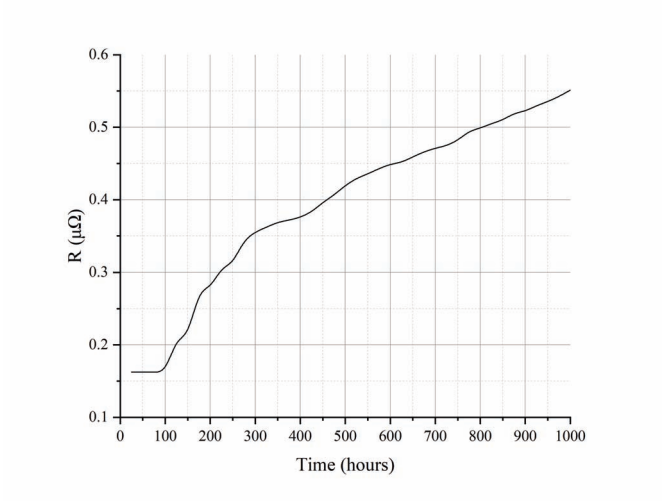

Fig. 6: Resistance over different experimental durations.

bump size significantly exacerbates EM effects. Fig. 8 shows the resistance of the reference and smaller model over time. Compared to the reference model, after 40 hours, EM phenomenon starts to occur on smaller models, and by reaching 500 hours, the resistance grows from 0.2386 $\mu\Omega$ to 0.8361 $\mu\Omega$, which is a 250% increase compared to 158% for the reference model. The reduction in model size leads to a larger resistance and higher current density, and the smaller bump experiences increased electron wind force, accelerating atomic migration.

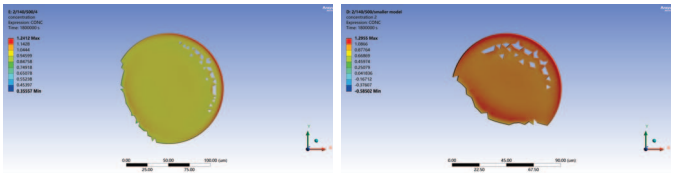

(a) reference (b) smaller model

Fig. 7: Simulation results for different model sizes.

The edge region of the birth/death element layer in the smaller model exhibits concentrated current flow, which results in current crowding, leading to enhanced Joule heating and a local temperature rise as shown in Fig. 9, accelerating the EM effect. This finding suggests that reducing bump dimensions without appropriate countermeasures (e.g., optimizing under-bump metallurgy or using barrier layers) may critically impact device reliability.

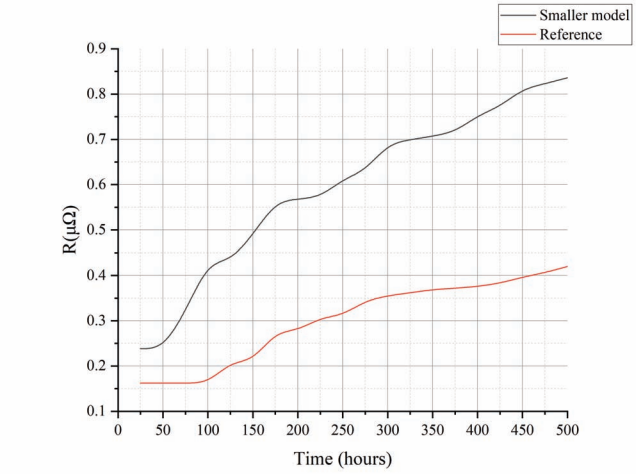

Fig. 8: Resistance for different model sizes.

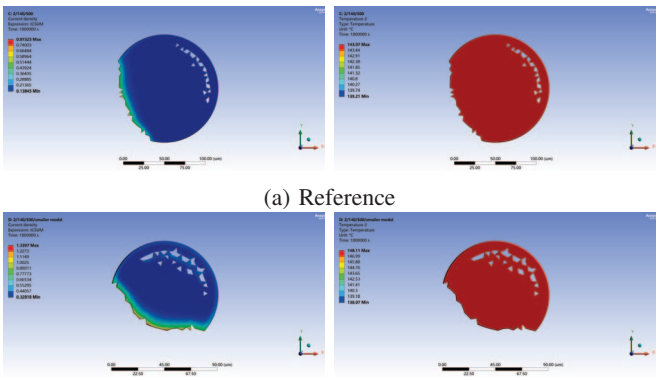

(a) Reference

(b) Smaller models

Fig. 9: Current density and temperature for different model sizes.

C. Temperature

Fig. 10 shows the simulation results of the layer at 2A, 100/120/140/160°C after 500 hours. Fig. 11 shows the resistance of the layer under different temperature over time. At 100°C, after 500 hours, EM does not occur in the birth/death element layer, and at 120°C after 500 hours, EM begins to occur. At 160°C, EM begins to occur after 50 hours, by reaching 500 hours, the resistance grows from 0.1624 $\mu\Omega$ to 0.5824 $\mu\Omega$, which is a 258% increase. According to the **Black's Equation**,

$$MTTF \propto J^{-n} e^{\frac{E_a}{kT}}$$

the rise in the temperature T leads to an exponential decrease in the MTTF and increases atomic migration rate, leading to faster EM-driven void formation and significant lifetime shortened. At the same time, thermal stress at different temperatures will also affect the deformation of the element. Stress concentration is more likely to form at high temperatures, accelerating the formation and expansion of cracks and voids.

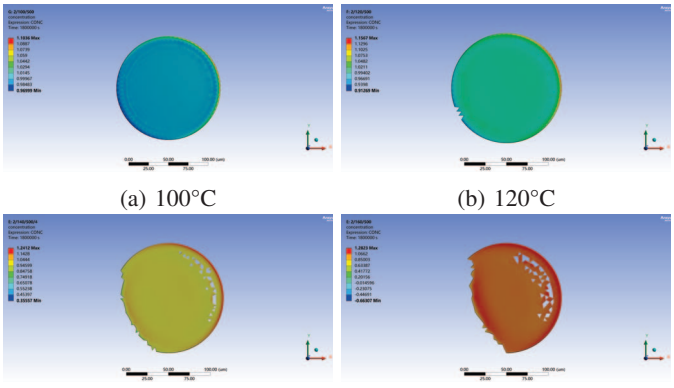

(a) 100°C (b) 120°C

(c) 140°C (d) 160°C

Fig. 10: Simulation results for different temperature.

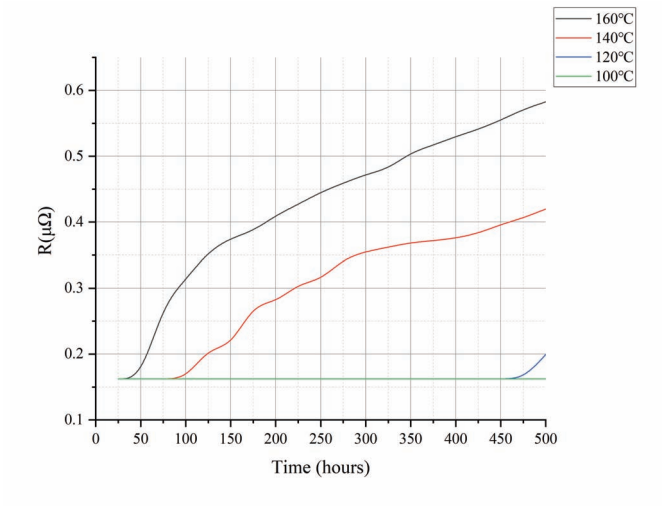

Fig. 11: Resistance for different temperature.

D. Current density

Fig. 12 shows the simulation results of the layer at 1/2/4 A, 140°C after 500 hours. Fig. 13 shows the resistance of the layer under different current densities over time. The larger current density increases the migration rate of metal atoms with the electron wind, which accelerates the formation of voids and the evolution of cracks, and aggravates the EM phenomenon. At 4 A, EM begins to occur after a few hours, by reaching 500 hours, the resistance grows from 0.1624 $\mu\Omega$ to 0.515 $\mu\Omega$, which is a 217% increase.

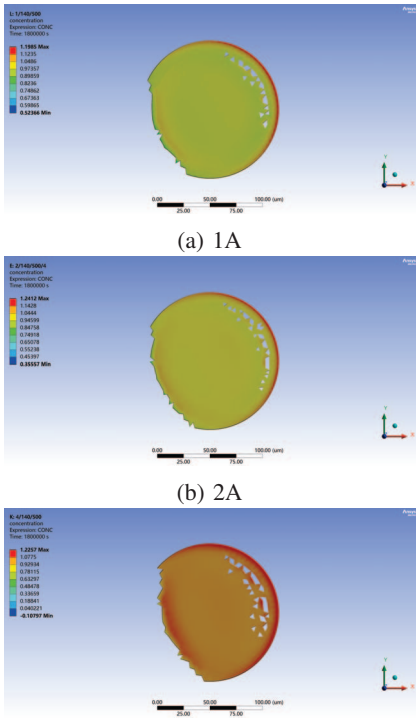

(a) 1A

(b) 2A

(c) 4A

Fig. 12: Simulation results for different current densities.

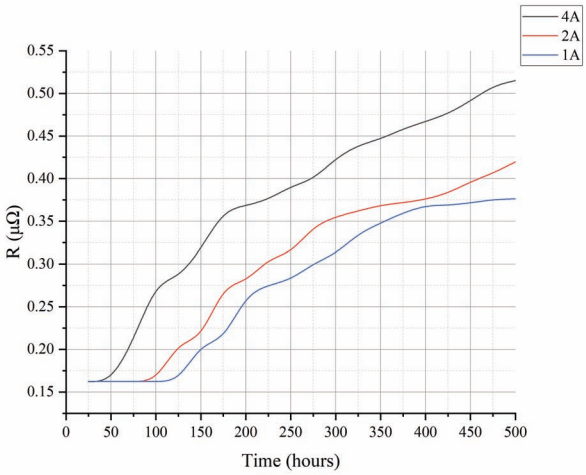

Fig. 13: Resistance for different current densities.

E. Inverse current density

When an inverse current is applied, the position of the birth/death element layer, i.e., the region where EM occurs is redefined. Fig. 14 shows the change of cross-section and the constraints for the inverse current simulation. Fig. 15 shows the simulation results of the layer at -1/2/4 A, 140°C after 500 hours. Fig. 16 shows the resistance of the layer under different inverse current densities over time. When inverse currents are applied, a different EM mechanism is observed. Due to the difference in the defined position of the birth/death element

layer, the difference in the interface area and properties causes a change in the distribution of the current density, and the formation of voids and the propagation of cracks under the inverse current is more like abrupt failures and shows a tendency to develop from the periphery to the center than that of the forward current. The inverse currents lead to faster formation of EM-induced voids and the magnitude of the inverse current has less effect on the starting point compared to the forward current. Even at -1 A after tens of hours, the EM also leads to an increase in resistance. At -4 A, after 500 hours, the resistance grows from 0.3674 $\mu\Omega$ to 0.5584 $\mu\Omega$, which is a 52% increase. The initial resistance of the birth/death element layer under the inverse currents is higher than that of the forward current, indicating a different atomic redistribution pattern. The solder bump has a larger contact area with Cu pad, alleviating the current crowding effect, which shows the increase in resistance with time is smaller, indicating that the model has a good resistance to EM for the inverse current.

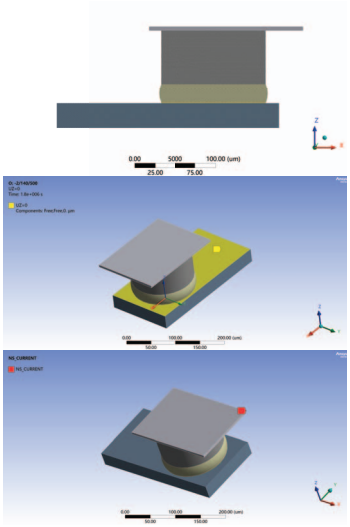

Fig. 14: Cross-section and the constraints for the inverse current simulation.

F. Discussion

In this paper, the birth/death element method is used to simulate the EM phenomenon of the model under different experimental times, model sizes, temperatures, and current. However, the birth/death element method can only be performed in the defined layers, and the simulation cannot fully take into account the influence of the entire model. For example, there is a large current crowding phenomenon at the contact corner between the Cu pillar and the upper Al pad. In future work, the EM phenomenon in this contact area can also be studied. The birth and death element method also has the problem of residual stress. The stress redistribution caused by the removal of the element may lead to unrealistic simulation results [7]. The stiffness value of the element removed from the birth/death element layer needs to be set low enough to reduce interference with the calculation results, but too low may

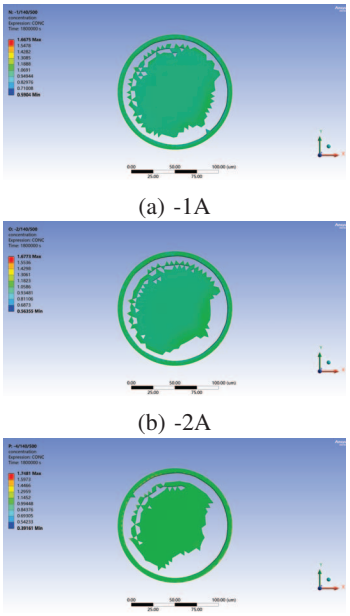

(a) -1A

(b) -2A

(c) -4A

Fig. 15: Simulation results for different inverse current densities.

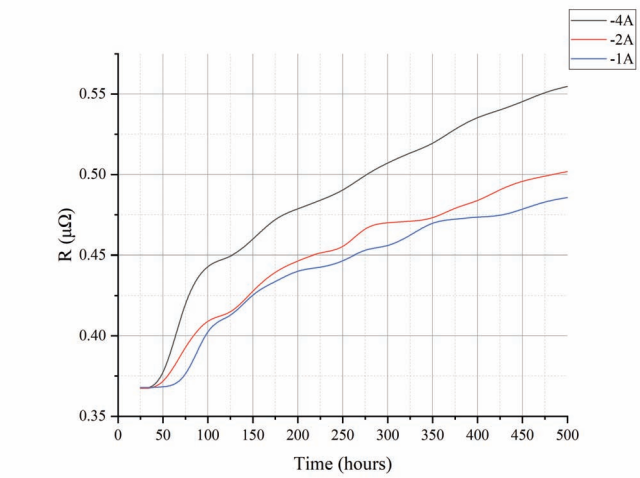

Fig. 16: Resistance for different inverse current densities.

cause numerical instability and non-linear problems cannot converge. The simulation accuracy is highly dependent on the quality and resolution of the mesh, but too fine a mesh can easily cause some elements to deform too much and cannot be solved. In this simulation, if the time step is reduced and the number of substeps is increased, the element size can be further refined to pursue better mesh independence and more accurate calculation results, but as mentioned earlier, this is a balance between efficiency and accuracy.

V. CONCLUSION

This study used the birth-death element method in ANSYS to investigate the EM behavior of Cu pillar bump structures

in 3D integration. Simulation results show that higher temperature and higher current density significantly accelerate atomic migration, leading to void formation and increased resistance, posing the risk of open circuit failure. The reduction in bump size exacerbates the current crowding effect and exacerbates EM-induced failures. It is worth noting that the inverse current density causes a slower resistance growth rate compared to the forward current, presenting a different formation mechanism of EM-induced voids. These findings provide a method to study the failure mechanisms and predict life of packaging structures in 3D intergration, which can help optimize the Cu pillar bump design to improve EM resistance performance, thereby improving the reliability and life of advanced packaging technology.

REFERENCES

[1] B.-H. Kwak, M.-H. Jeong, and Y.-B. Park, "Effects of temperature and current stressing on the intermetallic compounds growth characteristics of cu pillar/sn–3.5ag microbump," Japanese Journal of Applied Physics,vol. 51, p. 05EE05, may 2012.

[2] K. Son, H. Ryu, G. Kim, J. Lee, and Y.-B. Park, "EM polarity effect of cu/ni/sn-ag microbumps for three-dimensional integrated circuits," in 2017 IEEE 19th Electronics Packaging Technology Conference (EPTC), pp. 1–3, 2017.

[3] E. E. Antonova and D. C. Looman, "Finite Elements for EM Analysis," 2017 IEEE 67th Electronic Components and Technology Conference (ECTC), Orlando, FL, USA, 2017, pp. 862-871, doi: 10.1109/ECTC.2017.310.

[4] S. ZHAO, F. QIN, M. YANG, M. XIANG and D. YU, "Study on warpage evolution for six-side molded WLCSP based on finite element analysis," 2019 20th International Conference on Electronic Packaging Technology(ICEPT), Hong Kong, China, 2019, pp. 1-4, doi: 10.1109/ICEPT47577.2019.245281.

[5] Maoyu Li, Yuanhao Huang, Zikai Hua and Jianhua Zhang, "Finite element analysis of laser bonding process on organic light-emitting device," 2010 12th Electronics Packaging Technology Conference, Singapore, 2010, pp. 190-194, doi: 10.1109/EPTC.2010.5702631.

[6] L. Yang, J. Gong and C. Yue, "Thermal Deformation Analysis for Power Device During the Reflow Process," 2024 25th International Conference on Electronic Packaging Technology (ICEPT), Tianjin, China, 2024, pp. 01-05, doi: 10.1109/ICEPT63120.2024.10668667.

[7] Y. Jiang et al., "MCP Bottom Die Crack Issue during Destructive Analysis," 2007 9th Electronics Packaging Technology Conference, Singapore, 2007, pp. 864-868, doi: 10.1109/EPTC.2007.4469685.

[8] Kwaśniewski, L.. (2013). Application of grid convergence index in FE computation. Bulletin of the Polish Academy of Sciences: Technical Sciences. 61. 10.2478/bpasts-2013-0010.